The role of type II F_B(I): Tl$^+$ defect in laser light generation and color image formation at the low coordination surface sites of AgBr : ab initio calculations

A.S.Shalabi * and A.S.Algaber,

Department of Chemistry, College of Science, Qatar University,
P.O.Box 2713, Doha, Qatar

N.K.Madi
Department of Physics, College of Science, Qatar University,
P.O.Box 2713, Doha, Qatar

Kh.M.Eid and Z.M.Fathy

Department of Physics, Faculty of Education, Ain Shams University,
Cairo, Egypt

Abstract

The role of type II F_B (I):Tl$^+$ color center at low coordination surface sites of AgBr thin films in providing tunable laser activity and photographic sensitization is examined. The double-well potential at this site is investigated using ab initio molecular electronic structure calculations. Clusters of variable sizes were embedded in simulated Coulomb fields that closely approximate the Madelung fields of the host surfaces, and ions that are the nearest neighbors to the F_B defect site were allowed to relax to equilibrium in each case. The calculated Stokes shifted optical transition bands suggest that laser activity is relatively weak and fades quickly as the coordination number of the surface ions decreases from 5(flat) to 4(edge) to 3(corner). An attempt has been made to explain these results in terms of Madelung potentials and optical-optical conversion efficiencies. All relaxed excited states of the defect containing surfaces were deep below the lower edges of the conduction bands of the ground-state defect-free surfaces indicating that type II F_B (I):Tl$^+$ is suitable laser defect. The probability of orientational destruction of the two centers, attributed to the assumed saddle point ion configurations along the <110> axis, was found to decrease as the coordination number of the surface ions decreases. The possibility of exciton (energy) transfer between sites of different coordination numbers was clarified. The Glasner-Tompkins empirical relation was generalized to include type II F_B (I):Tl$^+$ doped surfaces. As far as photographic sensitization is concerned, a supersensitizer increases the sensitizing capabilities of the two examined dye molecules by increasing the relative yield of quantum efficiency Φ. F_A sensitizes the low coordination surface sites of the defect free AgBr by lowering the bottoms of the conduction bands. The difference in the sensitizing capabilities between the two examined dyes was estimated by calculating the quasi Fermi levels.

1. Introduction

The F_B center consists of an F center associated with a pair of impurity cations. Two categories of F_B centers exist-differing in their relaxation behavior. Type I F_B centers [1] are formed if the two impurity cations neighboring the F center lie on the same <100> crystal axis. This center has F like optical properties and is not laser active. In type II F_B centers [2] the two impurity cations are positioned on different <100> axes with respect to the F center forming a triangular configuration. Only this latter arrangement allows the formation of a saddle point configuration after optical excitation with a relaxed excited state lowered well below the conduction band and an electric dipole emission with Stokes shift.

As far as laser light generation is concerned, the electron-phonon coupling provides the most important property of broadened Stokes-shifted optical transition bands between absorption and emission and an almost ideal four energy level scheme [3]. The electrons associated with a defect interact strongly with the surrounding vibrating crystal ions, resulting in optical transitions, which are allowed in a broad band around the defect specific central transitions. The possible energy level structure of an F_B center electron is influenced by the shape and depth of the electronic binding potential. This potential is determined mainly by the distance and geometrical arrangement of the nearest surrounding lattice ions, which oscillate around their equilibrium positions. The ionic equilibrium is different for different electronic states and the electron phonon coupling and its effect on the optical transitions can be illustrated with a well-known type of configuration coordinate diagram [4].

When we come to consider the simple F center, the excited wave function in the relaxed excited states starts to overlap with the ground state wave function of other F centers at concentrations of about 10^{16} cm^{-3}. This causes a strong radiationless decay. In addition, transitions from the relaxed excited state into close-lying conduction band can occur. As a consequence of these losses, the kind of F center that readily produced in several hosts is not suitable as laser active material. The development of color center lasers therefore depends on the testing of known color center systems with more favorable optical properties, and the development of new laser active defects. It appears that a laser suitable defect should have the following properties: (1) one electron defect center (2) compact electronic states (3) relaxed excited state deep below the conduction band, and (4) possible experimental production of the center in high concentrations ($\geq 5 \times 10^{16}$ cm^{-3}). A well-controlled production of laser crystals requires irradiation of the crystals below the temperature range of anion vacancy mobility in a first step. We have therefore calculated the relaxed excited state orientational destruction of the present F_B center, hopefully to resolve problems related to the experimental production of this center in high concentrations.

In general, ab initio calculations of laser light generation at the ionic crystal surface is still lacking, and until recently the potential of F_B center for useful laser action at the surface of AgBr has been ignored. We have therefore made an attempt to examine type II F_B (I):Tl$^+$ laser action at the low coordination surface sites of AgBr.

Other energetic properties such as relaxation energy, exciton (energy) transfer, and Glasner-Tompkins empirical rule have been examined too.

As far as color image formation is concerned, silver halide photography contains several unique phenomena. These include characterization of silver halide micro- and macro-crystals, characterization of silver halide micro-clusters as latent image and sensitization centers, the relationship between electronic and molecular structure of sensitizing dyes and light induced electron transfer from sensitizing dyes to silver halide. The traditional silver halide photographic process is still superior in image quality for use in many applications. The unique physical properties of silver halides are behind their unique utilities in photographic development. Despite the great advances in film quality and sensitivity, the theoretical framework describing the elementary acts of the photographic process at the atomic level has been taking shape much more slowly. In 1988, Hamilton [5] reported that the light-sensitive elements of conventional photographic materials are crystallites principally of the bromide or chloride salts of silver. Absorption of a few photons results in the reductive formation of one or more clusters of silver atoms on the surface. These clusters act as catalysts to promote further reduction of the host crystallites during photographic development. The success of the system depends upon the particular physical properties of the silver halides, such as their bonding and electronic structure, the dielectric properties, the point defect structure and the electronic transport characteristics. Hamilton reviewed all these and followed the ways in which they interact to lead to the favorable photodecomposition in some details. More recently, in 1990, Flad, et al. [6] investigated the alternating process of adsorption of Ag^+ and trapping of a photoelectron on a (100) AgBr surface by quantum mechanical calculations. Their results gave some insight into the initial steps of the photographic process, namely, absorption of two photons which lead to the formation of a sublatent image. In 1993, Shelimov, et al. [7] carried out ab initio calculations of the geometry, electronic structure, ionization and excitation energies of M-center on the AgBr (100) surface. They reported that the structure, formed in the process of surface reduction, may be viewed as Ag_2 molecule adsorbed on the AgBr (100) surface with a "pit" and may become a primary center for photographic latent image formation. In 1995, the textbook of Tani [8] provided the developments in photographic sensitivity, image quality and other capabilities of imaging systems. In 1999, Malik, et al. [9] constructed theoretical models based on experimental data for AgBr(100) surface with ledge and kink type point defects. Their theoretical models provided a mechanism for the formation of a latent subimage through trapping photoelectrons and subsequent pairwise distortion of the surface silver. In the same year, 1999, Hailstone [10] used computer simulation to study the effect of iodide impurity on silver cluster formation on AgBr microcrystals. In 2001, Shalabi, et al. [11] examined the F_2 and F_2^+ models of photographic sensitization at the thin surface film of AgBr.

When a photographic film is exposed to light, on average about 8-12 absorbed photons per crystal, it is said to bear a *latent image* that is capable of being converted to a *visible image* by a developer. The image formed is either black and white or color. In the process of color image formation, electron transfer takes place from optically excited dye molecules (sensitizing dyes) to the conduction band of silver halides. Sensitizing dyes are thus required to have the abilities to absorb light at a desired wavelength and to transfer electrons to the conduction band of silver halides from their excited states. The role of irregular surface defects, such as ledge or kink

type defects, in latent image formation has been the subject of several investigations [12]. It has been postulated that these sites are places where a latent image cluster could preferentially form. However, less theoretical attention has been paid to the role of electron hole centers, such as F_B, in color image sensitization. It is therefore our intention to examine how electron transfer from a dye molecule in the excited state or the one electron surplus state under the effect of a supersensitizer to the bottom of the conduction band of a silver bromide surface, in the process of color image formation depends on type II $F_B(I):Tl^+$ defect, using ab initio methods of molecular electronic structure calculations.

The present study is organized as follows: Section 2 gives a brief account of the theoretical methods, namely, simulation of the low coordination surface of silver bromide, by configuration interaction singles method, configuration coordinate diagrams and density functional theory calculations, is given. In Section 3, the results of the double-well potentials of type II $F_B(I):Tl^+$ defect, namely, color center laser generation and color image sensitization, are given and discussed. Finally, the results were concluded and collected in Section 4.

2. Methods
2.1 Crystal simulation

There are several methods to simulate crystals, either by finite or infinite systems. In the case of finite systems, only local portions of the crystal are considered. For such an approach, clusters of varying sizes in bulk structure are suitable approximations. Here one may distinguish between free clusters, saturated clusters and embedded clusters. Free clusters are simply parts of the bulk, and their simulations should work best if the structures of the stable clusters and of the bulk are very similar. Since free clusters have rather large closed surfaces due to the many surface sections around the outer cluster atoms it seems advantageous to saturate the free valence at all sites which are not supposed to represent the real crystal. This saturation can be achieved by simulation with real atoms or pseudo-atoms. Alternatively, the free cluster can be embedded in an electric field of point charges, which are an approximate account of the rest of the bulk. In the case of infinite systems, the influence of the bulk can be taken into account by point charges rather than by atoms. This procedure can be used for ionic crystals with atoms of alternating charges. An approach, which preserves the translational invariance of ideal crystals, is the primitive unit cell method. This method uses Block functions with many wave vectors, **k**, to account for the translational periodicity of the unit cell. However, instead of using complex wave functions it is possible to restrict the calculations to **k**=0 in **k** space, and enlarge the unit cell instead [13]. It is common to most applications of these approaches that they restrict themselves to a slab consisting of two or several layers for the representation of the bulk, and this usually suffices to generate a good surface [14]. Early studies by Kunz and co-workers [16p4ws] and by Clobourn and Mackrodt [15] used clusters that were terminated by ionic charges and the choice of the appropriate charges for the point ions has been discussed for an fcc structure like MgO [16]. In the ab initio model potentials method [19p4ws] the metal oxide clusters are first embedded, then the rest of the crystal is taken to be ionic charges.

2.1.1 Bulk simulation

To simulate the AgBr crystal bulk, we follow a procedure previously reported for LiH [17], LiF and NaH [18], MgO [19] and AgBr [20]. A finite AgBr crystal of 288 point charges was first constructed. The Coulomb potentials along the X and Y axes of this crystal are zero by symmetry as in the host crystal. The ±1 charges on the outer shells listed in Table 1, were then modified, using a fitting procedure, to make the Coulomb potential at the four central sites closely approximates the Madelung potential of the host crystal, and to make the Coulomb potential at the eight points with coordinates $(0,\pm R,\pm R)$ and $(\pm R,0,\pm R)$ where R is half the lattice distance, which for AgBr is 2.887 A^o, equal to zero as it should be in the host crystal. With these charges, 0.409283 and 0.800909, the Coulomb potential in the region occupied by the central ions is very close to that in the unit cell of the host crystal. The Coulomb potential was calculated to be 1.748 at each of the four central sites, compared with 1.746 for an alkali halide ionic crystal, and 0.0 at each of the previously defined eight points, compared with 0.0 for an ionic crystal.

2.1.2 Surface simulation

The low coordination surface sites of the AgBr crystal represented in Fig.1 were generated as follows:

1. all charged centers with Cartesian coordinates $(\pm X)$, $(\pm Y)$ and $(Z>0)$ were eliminated to generate a flat surface with 176 charged centers occupying the three dimensional space $(\pm X)$, $(\pm Y)$ and $(Z\leq 0)$

2. all charged centers with Cartesian coordinates $(X<-1)$, $(\pm Y)$ and $(Z>0)$ were eliminated to generate an edge with 121 charged centers occupying the three dimensional space $(X\geq -1)$, $(\pm Y)$ and $(Z \leq 0)$

3. all charged centers with Cartesian coordinates $(X<-1)$, $(Y>1)$ and $(Z>0)$ were eliminated to generate the Br$^-$ corner with 81 charged centers occupying the three dimensional space $(X\geq -1)$, $(Y\leq 1)$ and $(Z\leq 0)$.

The clusters of Fig.2 were then embedded within the central region of the crystal surface. All the electrons of the embedded clusters were included in the Hamiltonians of the *ab initio* calculations. Other crystal sites entered the Hamiltonians either as complete or partial ionic charges as demonstrated in Table 1.

2.2 Calculations
2.2.1 Configuration Coordinate diagrams

The geometric relaxation of F_B center in the ground and excited states is a key quantity for laser activity due to vibrational coupling. In other words, the possible energy level structure of F_B center electron is influenced by the shape and depth of the electronic binding potential. This potential is determined mainly by the geometrical arrangement of the nearest surrounding lattice ions, which vibrate around their equilibrium positions. The ionic equilibrium is different for different electronic states, and the electron-phonon coupling and its effect on the optical transitions can be illustrated with a configuration coordinate diagram [21]. In the configuration coordinate diagram, the electronic energies in the ground and excited states are plotted versus the configuration coordinate Q which represents a certain localized mode or normal mode of the lattice coupling to the electron. In other words, Q represents the simultaneous displacement of the nearest neighbor cations to the defect site from the lattice inter-ionic separation (Q=0.0) along the axes joining them with the defect site. This is called a linear coupling mode. The other ions were retained in their original positions in the lattice. Starting from the ground state of an F_B center an optical excitation produces a transition into the excited states at fixed nuclear coordinates assuming Franck-Condon principle i.e. vertical in the configuration coordinate diagram. Due to the Gaussian shaped probability function for the lowest vibrational state, the transition starts with highest probability from the equilibrium position Q_1. The electronic distribution reached after excitation is not in equilibrium with the lattice at Q_1. As a consequence the ions relax new equilibrium positions. The vibrational energy will be dissipated via anharmonicity into lattice phonons, and the lattice will reach the new equilibrium position Q_2, the relaxed excited state. After the mean life time the excited electron returns by a vertical emission process to the ground state, and the subsequent lattice relaxation completes the optical cycle [3].

To construct the configuration coordinate diagrams, the ion clusters representing the F_B centers at the flat, edge and corner surfaces of AgBr were first embedded in the three-dimensional arrays of point ions described in 2.1.1 The representation of the ion clusters considered in the calculations is given in Fig. 2. The absorption and emission energies were then calculated as the difference between the total energies of the ground and excited states. For this purpose the relevant potential energy curves were calculated, then according to the Franck-Condon principle the absorption energy was calculated as that for a vertical transition from the minimum of the relaxed ground state to the excited state. The luminescence energy was calculated in a similar manner. Stokes shifts were then calculated as the difference between absorption and emission energies.

$$\Delta E_{absorption} - \Delta E_{emission} . \qquad (1)$$

2.2.2 The Configuration Interaction-Singles method

The Configuration Interaction-Singles method was employed for the calculations of F_B laser activity, exciton (energy) transfer, and the relaxed excited state orientational destruction of F_B. The Configuration Interaction-Singles method uses the configuration interaction approach and models excited states as combinations of single substitutions out of the Hartree-Fock ground state. The CI-Singles theory is an adequate zeroth-order treatment for many of the excited states of molecules. Treatments of large molecular systems can be made affordable by the avoidance of integral storage and transformation, and thus the Configuration Interaction-Singles method has a wide range of applicability. A satisfactory exploration of potential energy surfaces and accurate electronic properties of excited states are possible by the use of an analytic Configuration Interaction-Singles gradients [22]. The method includes some electron correlation in the excited states, and it can provide reasonable accuracy for excitation energies in comparison with the simplest way to find the lowest relaxed excited state in wide gap insulators, namely, the self consistent field calculations of the triplet state [23].

2.2.3 The Density Functional Theory method

Density functional theory was employed for the calculating the differences between the band gaps and exciton bands (Glasner-Tompkins empirical rule) and photographic sensitization. The density functional theory calculations were performed using Becke's three-parameter exchange functional B3 with LYP correlation functional [24]. This hybrid functional includes a mixture of a Hartree-Fock exchange with DFT exchange correlation. Originally the functional B included the Slater exchange along with corrections involving the gradient of the density [25] and the correlation functional LYP is that of Lee, Yang and Parr, which includes both local and non-local terms [26].

2.2.4 The CEP basis sets

The Stevens, Basch and Krauss CEP basis sets [27] were employed in the calculations. In these compact effective potential CEP basis sets, double zeta calculations are referred to as CEP-31G and triple zeta calculations are referred to as CEP-121G. It may be noted that there is only one CEP basis set defined beyond the second row ,and the two basis sets are equivalent for these atoms. For the s- manifold, a quadruple zeta representation of Gaussian type orbitals was found to be necessary to obtain energies with 0.001-0.003 a.u. of large, even-tempered basis set results . For this size expansion ,little accuracy was lost by restricting the s- and p- basis sets for each atom to have a common set of expansions .For the d -manifold ,fit with three parameter gaussian-type orbitals yields eigenfunctions which are <0.001 a.u. different from large, even-tempered results. These potentials and basis sets have been used to calculate the equilibrium structure and spectroscopic properties of several molecules, and the results compared extremely favorably with corresponding all-electron calculations. All of the computations reported in this paper were carried out using Gaussian 98 system [28].

3 Results and Discussion
3.1 F_B Laser generation and related properties
3.1.1. F_B laser generation

The configuration coordinate data of type II F_B :Tl$^+$ centers at the low coordination surfaces sites of AgBr are given in Table 2 and the configuration coordinate curves are shown in Fig.3. The strength of the electron- phonon coupling as reflected by the shift in the equilibrium positions Q_2 –Q_1 and the value of Stokes shift between the ground state and the low lying excited state   follows the order : flat>edge>corner. In other words, type II F_B :Tl$^+$ laser fades quickly as the bromine coordination decreases from 5(flat) to 4 (edge) to 3 (corner).

Since the electron density localization in the vacancy is an important feature of the defect with potential laser applications, we have calculated the optical absorption and luminescence energies after adding Br functions on the Br vacancy of the F_B center. The strength of the electron- phonon coupling as reflected by the shift in the equilibrium positions Q_2 –Q_1 and the value of Stokes shift between the ground state and the low lying excited state follows the very same order: flat>edge>corner. This implies, again, that type II F_B :Tl$^+$ fades quickly as the bromine coordination decreases from 5(flat) to 4 (edge) to 3 (corner). However, the magnitude of a Stokes shift was significantly reduced under the effect of the addition of Br basis functions on the Br vacancy.

The strong dependence of the absorption and emission energies, and consequently Stokes shifts, on ion coordination is probably due to a combination of several factors. Some of them have already been discussed by Garrone, Zecchina, and Stone [**29**] and include the reduction of the Madelung potential at low-coordinated sites, which leads to their substantial relaxation with respect to ideal geometry and to strong electron-density redistribution. The reduction of the Madelung potential alone cannot quantitatively explain the experimental data. This is perhaps not surprising because, as is demonstrated in the calculations of Shluger et al. [23], both the degree of localization of the excited state and the nature of the excited state depend on its location. Strong localization of the excited states on certain sites makes the Madelung argument less applicable. On the other hand, when replacing a Ag$^+$ ion neighbor of a normal F_B center in AgBr by two metal impurity ions, the difference in electron affinity Δ of these two ions compared with the host ion can be expected to affect the gross features of the electronic structure. In other words, if the electron affinity of the impurity cations is smaller than that of the host cation, one can expect that the F_B center electron in the ground state will be more bound to the vacancy site.

With a small Stokes shift, the optical-optical conversion efficiency will be increased. On the other hand, the reabsorption of emitted light by other F_B centers will also be increased. If the negative effect of reabsorption is stronger than the positive effect due to the conversion efficiency, then F_B laser acivity will be decreased. Inspection of Table 2 reveals that the negative effect of reabsorption is expected to increase as the coordination number of the surface site decreases.

A laser-suitable defect should have relaxed excited states deep below the conduction band of the perfect crystal [3]. To examine this issue, we consider the band structure of AgBr surface, i.e, the positions of the one- electron defect levels with respect to the perfect surface bands. In Table 3, we present the tops of the valence bands and the bottoms of the conduction bands for the ground states of the defect free surfaces as well as the highest occupied molecular orbitals and the lowest unoccupied molecular orbitals for the relaxed excited states of the defect containing surfaces. As shown all excited states are below the lower edges of the conduction bands of the defect free surfaces implying that F_B is laser suitable defect.

3.1.2. Relaxed excited state orientational destruction

One consequence of the relaxed excited state saddle point ion configuration of F_B center is a temperature-independent ionic reorientation during the pump cycle, i.e, a change of the center axis into a perpendicular (equivalent) orientation. This effect can be understood from Fig. 4 where it is seen that after the emission process the assumed saddle point ion has a 50% chance of hopping to the <110> anion vacancy site opposite to its starting location. Therefore, if an F_B center system is excited in either one of its absorption bands with polarized light having its propagation direction parallel to a <100> axis and the electric field vector **E** parallel to a perpendicular <100> axis, the F_B centers excited by the **E**-vector will quickly switch to <100> directions where they are no longer excited and the system will become experimentally transparent for the excitation light [3].

To examine the relaxed excited state orientational destruction of F_B center theoretically, we have calculated the total energies of the original relaxed excited state configuration and the assumed saddle point ion configurations of type II $F_A(I):Tl^+$ at the low coordination surface sites of AgBr. The difference between the energies of these two configurations (the energy barrier to the orientational destruction of F_B in laser experiment) are given in Table 4, from which it is confirmed that the barrier to the migration of the bromide anion to the F_B vacancy site decreases as the coordination number of the surface site decreases. In other words, the orientaional destruction of F_B is least probable at the most laser active flat surface. Experimentally, in order to avoid orientational bleaching, the pump polarization and direction of propagation of the pump beam inside the crystal have to be chosen such that they are not parallel to a <100> direction.

3.1.4. Exciton (energy) transfer

The relative total energies of the excited states at different low coordination surface sites could be used as the first indicator of whether the exciton excited at a particular surface site will transfer to another site. In order to be able to compare the results for different shapes and sizes of quantum clusters, the relative energies of the excited states for different coordinations were estimated following the method of Shluger et al. [23]. The ionization energies **I** for the clusters were calculated using the configuration interaction singles method. Assuming the vacuum level for all systems considered, the ground state total energies were placed at –**I** as shown in Fig.5. Then

the energies of the excited states were located with respect to the defined positions of the ground states using the excitation energies. As can be seen from Fig.5, the excited state at the corner sites have the highest energies relative to the flat and edge sites. The excited state at the corner has higher energy than that at the flat surface, and the latter is higher than at the edge. In other words the relative energies at the low-coordination surface sites of AgBr are sensitive to F_B imperfection and there is a possibility for exciton transfer from the corner sites to the higher coordinated flat and edge sites. Cox and Williams [30] argued that the excited state at the surface have positive values. Our estimates suggest that it could have negative values in agreement with the estimates of Shluger et al. [23] for MgO.

3.1.5 The Glasner -Tompkins relation

Glasner and Tompkins [31] reported an empirical relationship between the principal optical absorption of F centers in solids and the fundamental absorption of the host crystal. The difference between the first exciton absorption energy E_X and the F band energy E_F was found to depend almost exclusively on the negative ion species. In other words, the Glasner-Tompkins empirical rule suggests that the energy difference between the fundamental absorption of an alkali halide and the F band is very nearly a function of only the halide species. Exciton band E_X, F band E_F, E_X-E_F and $<E_X$-$E_F>$ for twelve alkali halides have been reported by Malghani and Smith [32], and for LiH and LiF by Shalabi et al.[33]. The dependence of Glasner-Tompkins relation on the dopant cation and surface coordination number of MgO, KCl and AgBr has been reported by Shalabi et al. [17-20]. However no attempts have been made to clarify the dependence of Glasner-Tompkins relation on the coordination number of AgBr surface sites containing type II F_B(I):Tl$^+$ centers.

To apply the Glasner-Tompkins relation to an F_B center, we have to calculate the corresponding band gaps and exciton bands. A complete treatment **of** the host dependence of band gaps would involve theories of excitons [34] and defects [35] that take into account the band structure. Since this will be a major undertaking and well beyond our present goal, we use the simple electron transfer model of the fundamental optical absorption of ionic solids developed by Hilsch and Pohl [36]. This model, in its simplest form, explains the fundamental optical absorption E_X as the transfer of an electron from a negative ion to a neighboring positive ion both placed adjacent to the defect site. It seems likely that all color centers have perturbed excitons formed nearby [17-18]. We have therefore calculated E_X as the change in Coulomb energy, associated with the transfer of an electron from a bromide anion to a silver cation, both placed adjacent to the F_B center, and we calculate E_{FB} as the energy difference between the highest occupied molecular orbital and lowest unoccupied molecular orbital. The correlation between the bromide ion coordination, the F_B center and the energy difference between the exciton bands E_X and band gaps E_{FB} are given in Table 5. As one can see from Table 5, the results emphasize the dependence of the energy differences on the bromide ion coordination of an F_B center. The energy difference decreases as the bromide ion coordination decreases generalizing the Glasner-Tompkins relation to include the coordination number of surface ions with type II F_B(I):Tl$^+$ defect.

3.2. Color image sensitization

In order to form color images, photosensitive materials are required to be sensitive to the three primary colors, blue, green and red. Silver halide itself absorbs ultraviolet and blue light, and is thus sensitive only to blue light in the visible region [8]. Spectral sensitization is now widely used to render silver halides sensitive to wavelengths longer than that of blue light, such as green, red and infrared by use of sensitizing dyes [37]. It is now accepted [38] that spectral sensitization in silver halide photographic materials takes place according to the electron injection mechanism proposed by Gurney an Mott [39], i.e., the transfer of electrons from optically excited dye molecules to the conduction band of silver halide. In other words, sensitizing dyes are required to absorb light and to transfer electrons to the conduction band of silver halides from their excited states.

By far the majority of practical sensitizing dyes are of cyanine or merocyanine classes, consisting of a conjugated carbon chain linking cyclic end groups. In the ground states of such a molecule, the highest occupied molecular orbital HOMO is filled, and absorption of light promotes an electron to the lowest unoccupied molecular orbital LUMO, usually in a $\pi \to \pi^*$ transition. The energy levels involved are dependent on molecular structure, and most of the relationships are now well understood.

A feature of major practical importance is the spectral location of the maximum of the dye absorption band, which is a measure of the energy difference between the HOMO and LUMO energy levels. The spectral characteristics, however, give no direct information on the absolute positions of either of the two levels involved. Such information is obtained either by theoretical calculations [40] or experimentally by photoemission measurements [41] or more commonly by electrochemical studies of dyes in solution [42]. However, molecular electrochemical measurements are of questionable relevance to aggregate forms of dyes [5] and adsorption [43].

Most of the previous quantum mechanical calculations, with varying degrees of sophistication, have been directed toward the alternating pattern of energy levels for a linear chain of s^1 silver atoms in the gas phase with increasing length [44]. The most extensive were those of Baetzold [45] in which models of the defect sites of the support have been included. However, less theoretical attention has been paid to electron injection from the developer molecule in the process of black and white image formation and/or electron and hole injection from the excited dye molecule in the process of color image formation.

3.2.1 Supersensitization

Supersensitization may be defined as a phenomenon in which the relative quantum yield of spectral sensitization (Φ) of a primary dye (electron acceptor) is increased on addition of a secondary dye (electron donor) called a supersensitizer (SS). The HOMO of a supersensitizer should be higher in energy than the HOMO of the dye molecule to allow for electron transfer. There are two major mechanisms for supersensitization in photography. One of them is hole-trapping supersensitization,

and the other is aggregate partitioning supersensitizaton. In the present study, we focus our attention to the former, namely, hole-trapping supersensitization. In hole-trapping sensitization, electron transfer takes place from the LUMO of the excited dye molecule (Dye*) to the conduction band of silver halide. The improvement of Φ of a dye with insufficient energy gap between the LUMO of Dye * and the lower edge of the conduction CB of silver halide (ΔE) by hole trapping supersensitization has been explained by Gilman [46]. Consider a dye alone, with small Φ i.e the excited electron in Dye* is situated below the bottom of the conduction band of AgBr. When this dye is excited to give Dye* in the presence of SS, electron transfer will take place from SS to Dye* to give Dye$^-$. The energy level of the excited electron in Dye* will then raise by electron injection from SS, and the electron in Dye$^-$ could be situated above the bottom of the conduction band CB of AgBr, and transferred with high efficiency to AgBr [47]. The long life time of Dye$^-$ as compared with Dye* could be another cause for the efficient electron transfer from Dye- to the conduction band of AgBr [48].

Now, to examine the effect of a supersensitizer, we first carried out full geometry optimizations for two dye molecules at the semi empirical level of theory using AM1 Hamiltonian [49]. The optimal geometries were then used as input data for the density functional theory DFT/B3LYP calculations employing the CEP basis set. Using the DFT level of theory, the top of the valence band VB and the bottom of the conduction band CB of the defect free surface as well as the HOMOs and LUMOs of the defect containing surfaces were calculated. The skeletal representation of the two dye molecules 1 and 2 are shown in Fig. 6.a, and the optimal configurations, produced by MOLEKEL [50], are shown in Fig.6.b. The electronic energy level diagram showing hole trapping supersensitization of Dyes 1 and 2 by a supersensitizer (SS) is given in Fig.7. In Fig.7, Dye* and Dye$^-$ are Dyes in the lowest singlet excited state and in the one electron surplus state respectively. The top of the valence band VB and the bottom of the conduction band CB of the defect free surface of AgBr as well as the singly occupied molecular SOMOs and the lowest unoccupied molecular orbitals LUMOs of the defect containing surfaces are also shown together with the α and β spin states SOMOs of each Dye$^-$.

Two major conclusions may be drawn from Fig. 7: (i) the supersensitizer SS increases the sensitizing capabilities of Dyes 1 and 2 by increasing the relative yield of quantum efficiency Φ relative to the bottom of the conduction bands CBs of the defect free surfaces of AgBr (ii) F_A sensitizes the low coordination surface sites of the defect free AgBr by lowering the bottoms of the conduction bands CBs. This in turn implies that F_A increases the sensitizing capabilities of Dyes 1 and 2 as well as the effect of the supersensitizer SS.

3.2.2 Quasi Fermi levels and sensitizing capabilities

As shown in Fig. 7, all of the highest occupied molecular orbitals HOMOs of Dye1 and Dye 2 and the singly occupied molecular orbitals SOMOs of Dye*1, Dye*2, Dye$^-$1 and Dye$^-$2 lie above the tops of the valence bands VBs of the defect free surfaces of AgBr. This implies that the desensitizing reactions (positive hole injections from the dye molecules to the defect free surfaces) are not allowed. However, the HOMOs of Dye1 and Dye 2 lie below the SOMOs of the defect containing surfaces. This implies that the desensitizing reactions (positive hole injections from Dye1 and Dye2 to the defect containing surfaces) are allowed. To determine quantitatively the difference in

the sensitizing capabilities between Dye1 and Dye2, we have calculated the quasi Fermi levels from the relation [**51**]

$$[E_{HOMO} + E_{LUMO}]/2 \ . \quad (2)$$

Quasi Fermi levels were calculated to be about –0.134 Hartrees for Dye1 and –0.140 Hartrees for Dye 2. This confirms that Dye1 has greater sensitizing capability than that of Dye 2 in the absence of a supersensitizer.

Conclusions

Ab initio molecular electronic structure calculations have been carried out to examine two practically important applications for type II F_A(I):Tl+ color center namely, laser light generation and color image sensitization, at the low coordination surface sites of AgBr. Two commonly used methods, configuration interactions-singles and density functional theory, have been employed in the calculations and three ionic clusters, containing from 10- 22 atoms from the third to the fifth rows of the periodic table, have been embedded in the simulated Coulomb fields of the crystal surface. Relaxation to equilibrim was taken into account and the compact effective potential CEP basis sets were employed in the calculations. The examined F_B center was found to be a suitable laser defect. The F_B laser activity decreases as the coordination number of the surface ion decreases. As far as the process of color image formation is concerned, a supersensitizer was found to increase sensitizing capabilities of two examined dyes by increasing the relative yields of quantum efficiencies. The F_B center increases the sensitizing capabilities of the two dyes, by lowering the top of the valence band of the defect free silver bromide surface, and enhances the effect of the supersensitizer. Based on quasi Fermi levels, the sensitizing capabilities of the two tested dyes were differentiated. The double-well potentials of F_B color center at the low coordination surface sites of silver bromide has therefore become evident, and a search for other double-well potential defects is suggested for future investigations.

References

1. I.Schneider, Phys.Rev.B177(1969)1324
2. N.Nishimaki, Y.Matsusaka and Y.Doi, J.Phys.Soc.Japan 33(1972)1909
3.W.Gellermann, J.Phys. and Chem.Solids 52(1991)249
4. D.B.Fitchen, Physics of Color Centers (Edited by W.B Fowler), Chap.5.
   Academic Press, New York (1968).
5. J.F.Hamilton, Advances in Physics, 37(1988)359.
6. J.Flad, H.Stoll, A.Nicklass and H.Preuss, Z.Phys.D 15(1990)79.
7. K.B.Shelimov, A.A.Safonov and A.A.Bagatur'yants, Chem.Phys.Lett.,
   201(1993)84.
8. T.Tani, *"Photographic Sensitivity : Theory and Mechanisms"*, Oxford
   University Press, New York (1995).
9. Abds-Sami Malik, John T.Blair, William A.Bernet, Francis J.DiSalvo
   and Roald Hoffman, J.Solid State Chem., 146(1999)516.
10.R.K.Hailstone, J.Appl.Phys., 80(1999)1363.
11.A.S.Shalabi and Kh.M.Eid, J.Mol..Mod. 7(2001) 216.

A.S.Shalabi, T.F.El-Essawy, M.M.Assem, S.Abdel Aal and A.M.El-Mahdy, Physica B 315(2002)13.

12. L.E.Brady and J.F.Hamilton, J.Appl.Phys., 37(1966)2268.
  R.C.Baetzold, J.Phys.Chem.B 101(1997)8180.

13. S.Coluccia and L.Marchese, in International Symp. on Acid-Base Catalysis, edited by K.Tanabe, H.Hattori, T.Yamaguchi, and T.Tanaka Kodansha-Tokyo(1988).

14. W.S.Abdel Halim and A.S.Shalabi Solid State Commun. 124(2002)67.
  W.S.Abdel Halim and A.S.Shalabi, Appl.Surf.Sci. (2003) in the press

15. E.A.Colbourn and W.C.Mackrodt, Surf.Sci., 117(1982)571.

16. E.A.Colbourn, in: C.R.A.Catlow (Ed.), " *Advances in Solid State Chemistry*", Vol. I. JAI Press, London, 1999.

17. A.S.Shalabi, A.M.El-Mahdy, M.A.Kamel and H.Y.Ammar, Phys.B., 292(2000)59.
  A.S.Shalabi, Kh.M.Eid, M.A.Kamel and Z.M.Fathi, I.J.Modern Phys.C 11(2001)1491.

18. A.S.Shalabi, A.M.El-Mahdy, M.A.Kamel and G.H.Ismail, J.Phys. and Chem. Solids, 60(2001)1007.
  A.S.Shalabi, A.M.El-Mahdy, M.A.Kamel and H.Y.Ammar, Phys.B., 304(2001)444

19. A.S.Shalabi and A.M.El-Mahdy, J.Phys. and Chem.Solids, 60(1999)305.
  A.S.Shalabi and A.M.El-Mahdy, Phys.Lett.A 281(2001)176.

20. A.S.Shalabi and Kh.M.Eid, J.Mol..Mod. 7(2001) 216.
  A.S.Shalabi, T.F.El-Essawy, M.M.Assem, S.Abdel Aal and A.M.El-Mahdy, Physica B315 (2002)13

21. W.B.Fowler and D.L.Dexter, Chem.Phys. 43(1965)768.

22. J.B.Foresman, M.Head-Gordon, J.A.Pople and M.J.Frisch, J.Phys.Chem. 96(1992)135.
  J.B.Foresman and J.B.Foresman, Exploring Chemistry with Electronic Structure Methods, 2nd edition (Gaussian Inc., Pittsburgh, PA,1996).

23. A.L.Shluger, P.V.Sushko and L.N.Kantorovich, Phys.Rev.B 59(1999)2417.

24. A.D.Becke, J.Chem.Phys. 98(1993) 5648.

25. A.D.Becke, Phys.Rev.A 38(1988) 3098.

26. C.Lee, W. Yang and R.g.Parr, Phys.Rev.B 37 (1988) 785.
  B.Miehlich, A.Savin, H.Stoll and H.Preuss, Chem. Phys.Lett.157 (1989) 200.

27. W.Stevens, H.Basch and J.Krauss, J.Chem.Phys. 81(1984)6026.
  W.Stevens, M.Krauss, H.Basch and P.G.Jasien, Can. J.Chem.70(1992) 612.
  T.R.Cundari and W.J. Stevens, J.Chem.Phys. 98(1993)5555.

28. Gaussian 98, Revision A.6, M. J. Frisch, G. W. Trucks, H. B. Schlegel, G. E. Scuseria, M.A.Robb, J.R.Cheeseman, V.G. Zakrzewski, J.A. Montgomery, Jr.,R.E.Stratmann, J.C.Burant, S.Dapprich, J.M.Millam, A.D.Daniels, K.N. Kudin, M.C. Strain, O. Farkas, J. Tomasi, V. Barone, M. Cossi, R. Cammi, B.Mennucci, C. Pomelli, C. Adamo, S.Clifford, J. Ochterski, G. A. Petersson, P. Y. Ayala, Q. Cui, K. Morokuma, D. K.Malick, A.D.Rabuck, K. Raghavachari, J.B. Foresman, J.Cioslowski, J.V.Ortiz, B.B.Stefanov, G.Liu, A.Liashenko, P.Piskorz, I. Komaromi, R.Gomperts,R. L. Martin, D. J. Fox, T. Keith, M. A. Al-

Laham, C. Y. Peng, A. Nanayakkara, C. Gonzalez, M. Challacombe, P. M. W. Gill, B. Johnson, W. Chen, M. W. Wong, J. L.Andres, C. Gonzalez, M. Head-Gordon, E. S. Replogle, and J. A. Pople, Gaussian, Inc., Pittsburgh PA, 1998.

29. E.Garrone, A.Zecchina and F.S.Stone, Philos.Mag.B 42(1980)683.
30. A.Cox and A.A.Williams, Surf.Sci., 175(1986)782.
31. A.Glasner and F.C.Tompkins, J.Chem.Phys. 21(1953)1817.
32. M.S.Malghani and D.Y.Smith, Bull.Am.Phys.Soc., 36(1991)1681.
    M.S.Malghani and D.Y.Smith, J.Phys. and Chem.Solids, 53(1992)831.
33. A.S.Shalabi, A.M.El-Mahdy, Kh.M.Eid. M.A.Kamel and A.A.El-Barbary, Phys.Rev.B 60(1999)9377.
34. R.S.Knox, " Theory of excitons", Academic Press, New York,1963.
    V.G.Plekhanov, Phys.Rev.B 54(1996)3869.
    A.A.O.Connel-Bronin, Phys.Stat.Sol., 38(1996)1489.
35. G.F.Koster and J.C.Slater, Phys.Rev. 95(1954)1167; 96(1954)1208.
    J.H.Crawford and L.M.Slifkin(Eds.), " *Point defects in Solids*",
    Plenum, N.Y., 1972.
    W.Hayes and A.A.Stoneham, " *Defects and Defect Processes in Non-Metallic Solids* ", Wiley, New York, 1985.
    E.Kotomin, A.Popov, Nucl.Inst.Meth.B 141(1998)1 and references therein.
36. R.Hilsch and R.W.Pohl, Z.Phys., 57(1929)145; 59(1930)812.
37. W.West, P.B.Gilman, in" *The theory of Photographic Sensitivity*"
    Fourth **edition,** T.H.James edition, Macmillan, New York (1977)
    Chap. 10.
38. T.Tani, J.Imaging Sci., 34(1990)143
39. R.W.Gurney, N.F.Mott, Proc.R.Soc. London Ser. A,146,151 (1938).
40. M.Tamura and H.Hada, Photogr.Sci.Eng. 11(1967)82.
    T.Tani and S.Kikuchi, Photogr.Sci.Eng. 11(1967)129; T.Tani, ibid., 13(1969)231; ibid., **14(1970)63**; T.Tani, S.Kikuchi and K.Honda, ibid., 12(1968)80.
41. T.B.Tang, K.Seki, H.Inokuchi and T.Tani, J.Appl.Phys. 59(1986)5.
42. R.Large, "*Photographic Sensitivity*" edited by R.Cox, Academic Press, New York(1973).
43. R.C.Nelson and P.Yianoulis, Photogr.Sci.Eng. 22(1978) 2.
44. E.Moisar and F.Granzer, Photogr.Sci.Eng., 26(1982)1.
    J.F.Hamilton and R.C.Baetzold, Photogr.Sci.Eng., 25(1981)189.
45. [48] R.C.Baetzold, Photogr.Sci.Eng., 17(1973)78; ibid., 19(1975)11; ibid., 28(1980)15.
46. P.B.Gilman, Jr.Photogr.Sci.Eng., 18(74)418.
47. T.Tani, T.Suzomoto, K.Ohzeki, J.Phys.Chem., 94(1990)1298.
48. W.West and P.B.Gilman," The Theory of Photographic Process"
    Fourth edition, edited by T.H.James,Macmillan,New York(1977).
49. M.J.S.Dewar and C.H.Reynolds, J.Comp.Chem., 2(1986)140.
50. MOLEKEL 4.0, P.Flukiger, H.P.Luthi, S.Portmann, J.Webber,
    Swiss Center for Scientific Computing, Manno(Switzerland),2000.
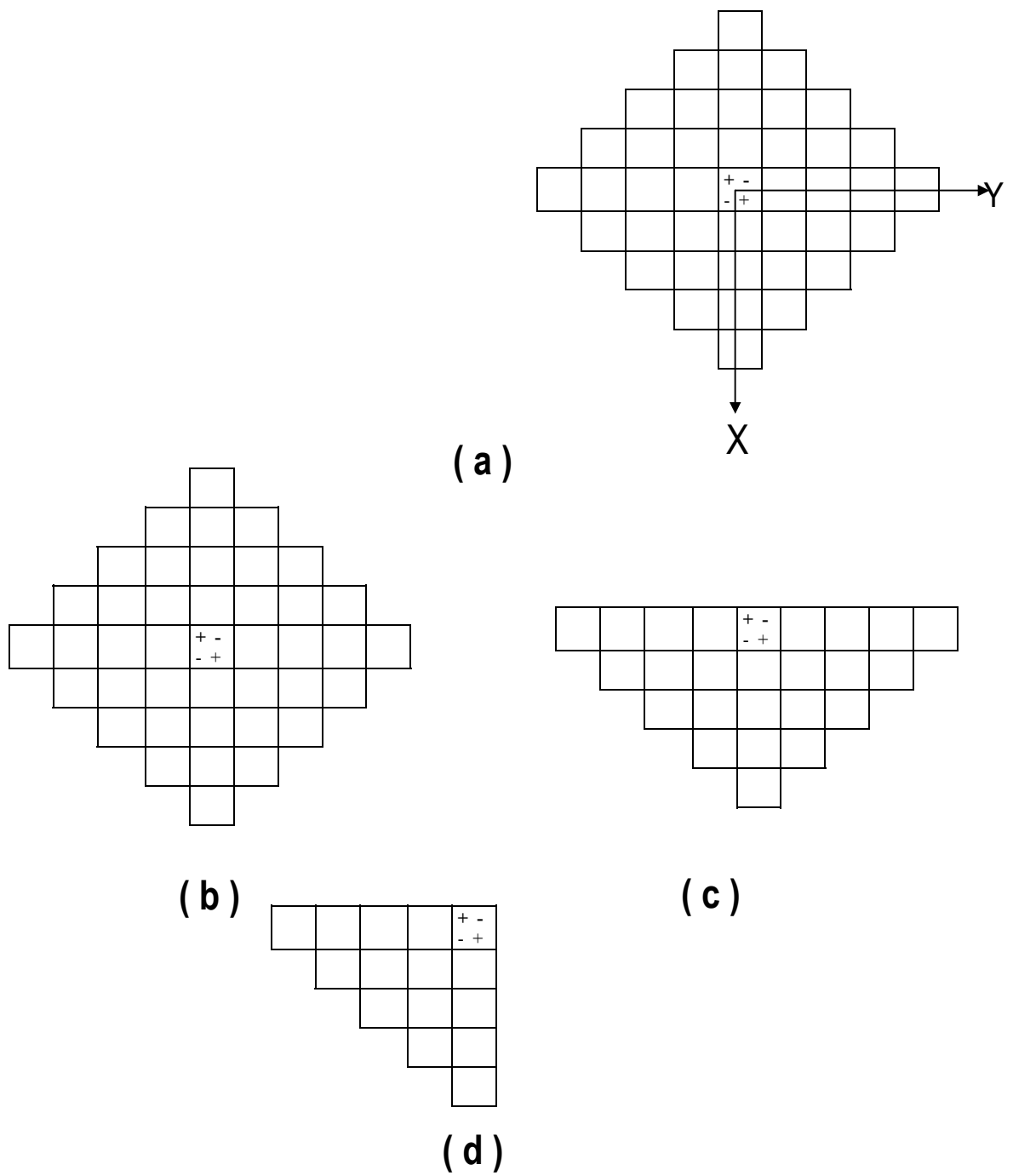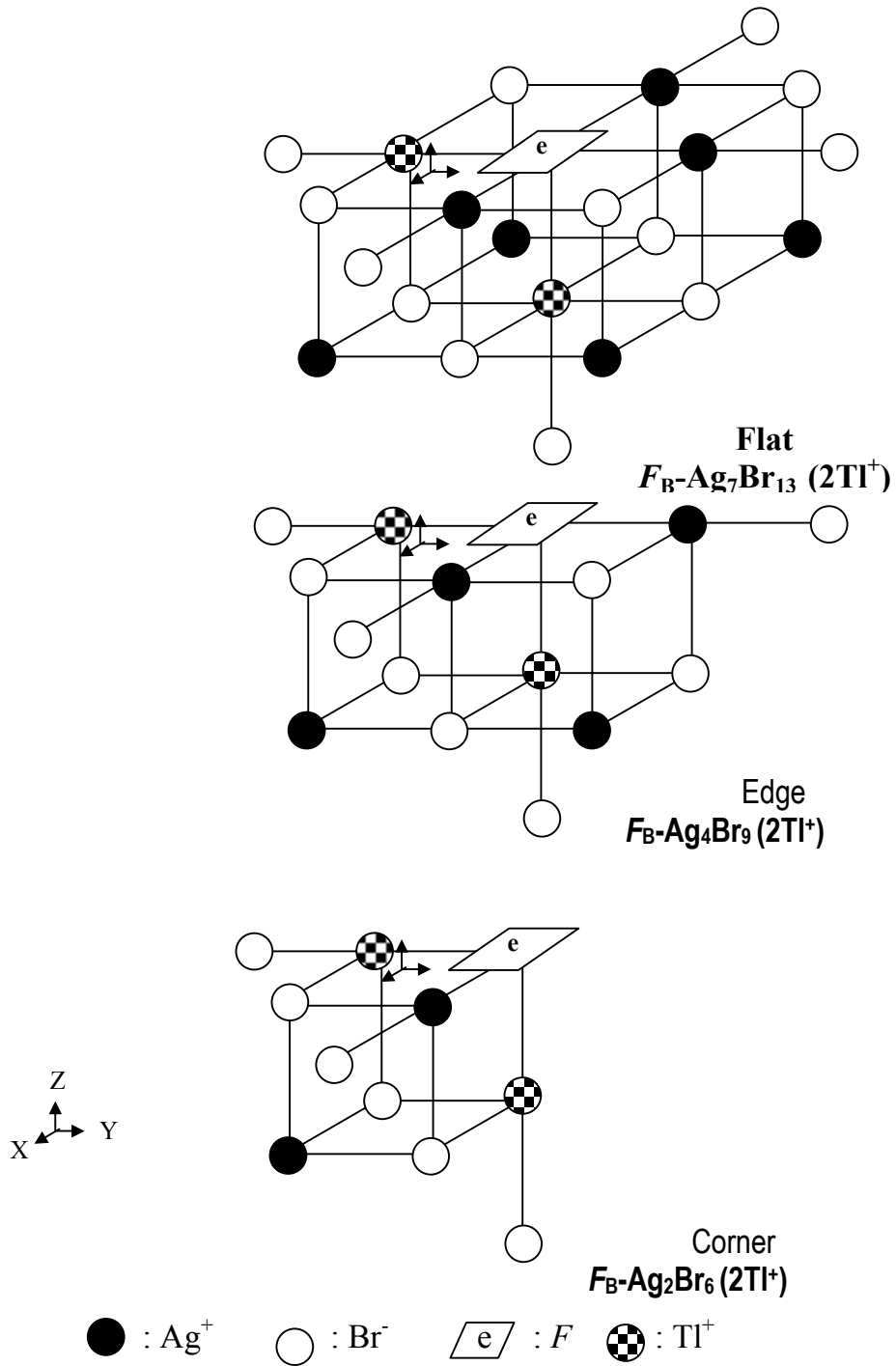51. T.Tani, Photogr.Sci.Eng., 18(1974)165.

Figure 1: Z = 0 plane representations of the AgBr crystal considered in the calculations.
(a) bulk (b) flat (c) edge (d) corner

Flat
F_B-Ag_7Br_{13} ($2Tl^+$)

Edge
F_B-Ag_4Br_9 ($2Tl^+$)

Corner
F_B-Ag_2Br_6 ($2Tl^+$)

● : Ag^+ ○ : Br^- [e] : F ⬡ : Tl^+

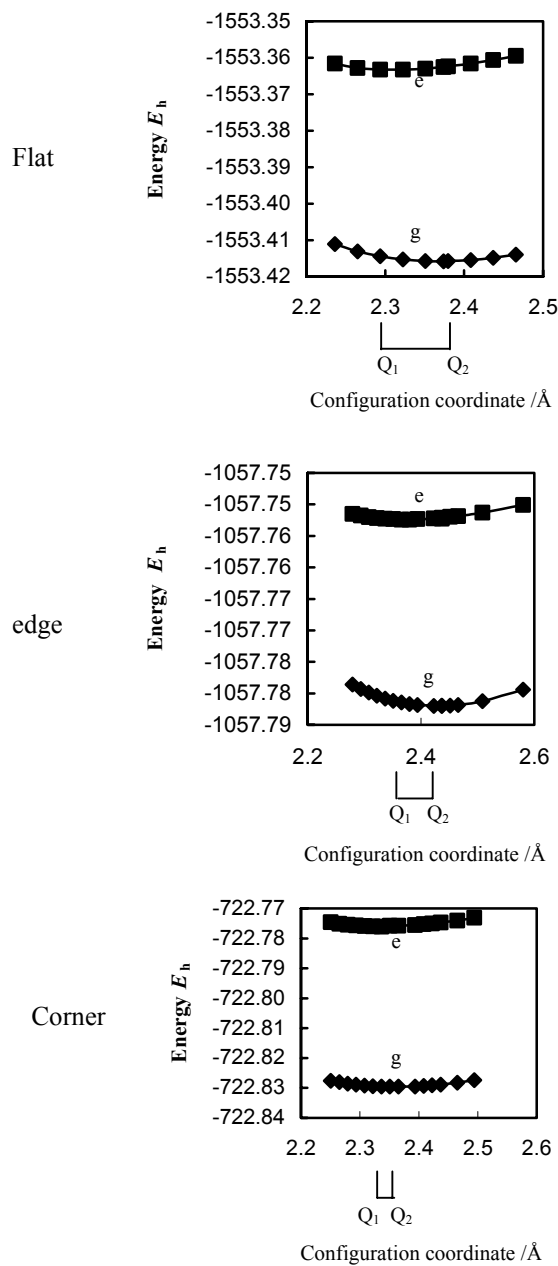**Figure (2): The low coordination surface clusters which are considered in the calculations.**

Figure (3) : The configuration coordinates diagrams of the low coordination
surfaces of AgBr with type II $F_B(I):Tl^+$ center.
Q₁: Minima of the ground state   Q₂: low lying excited states
g : ground state   e : excited states

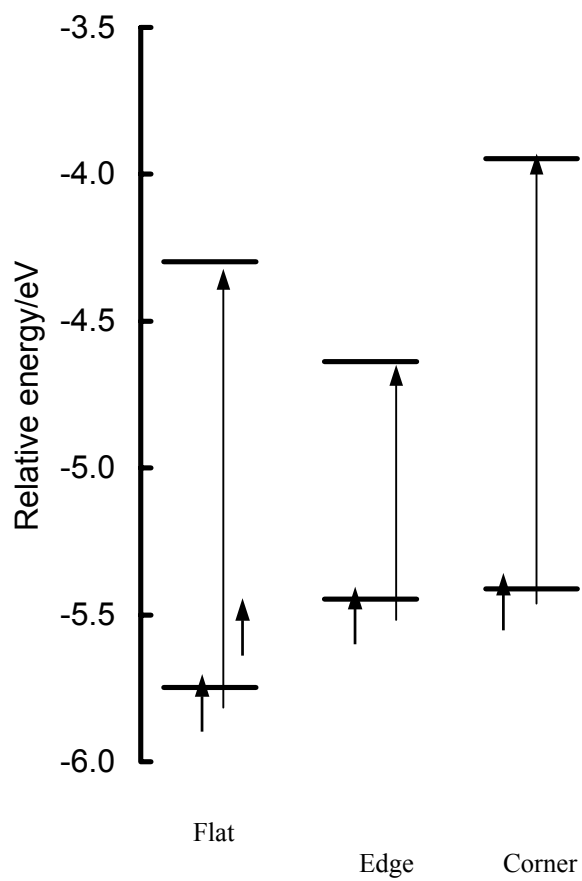Figure (4): Representation of the relaxed excited state saddle point
ion configuration

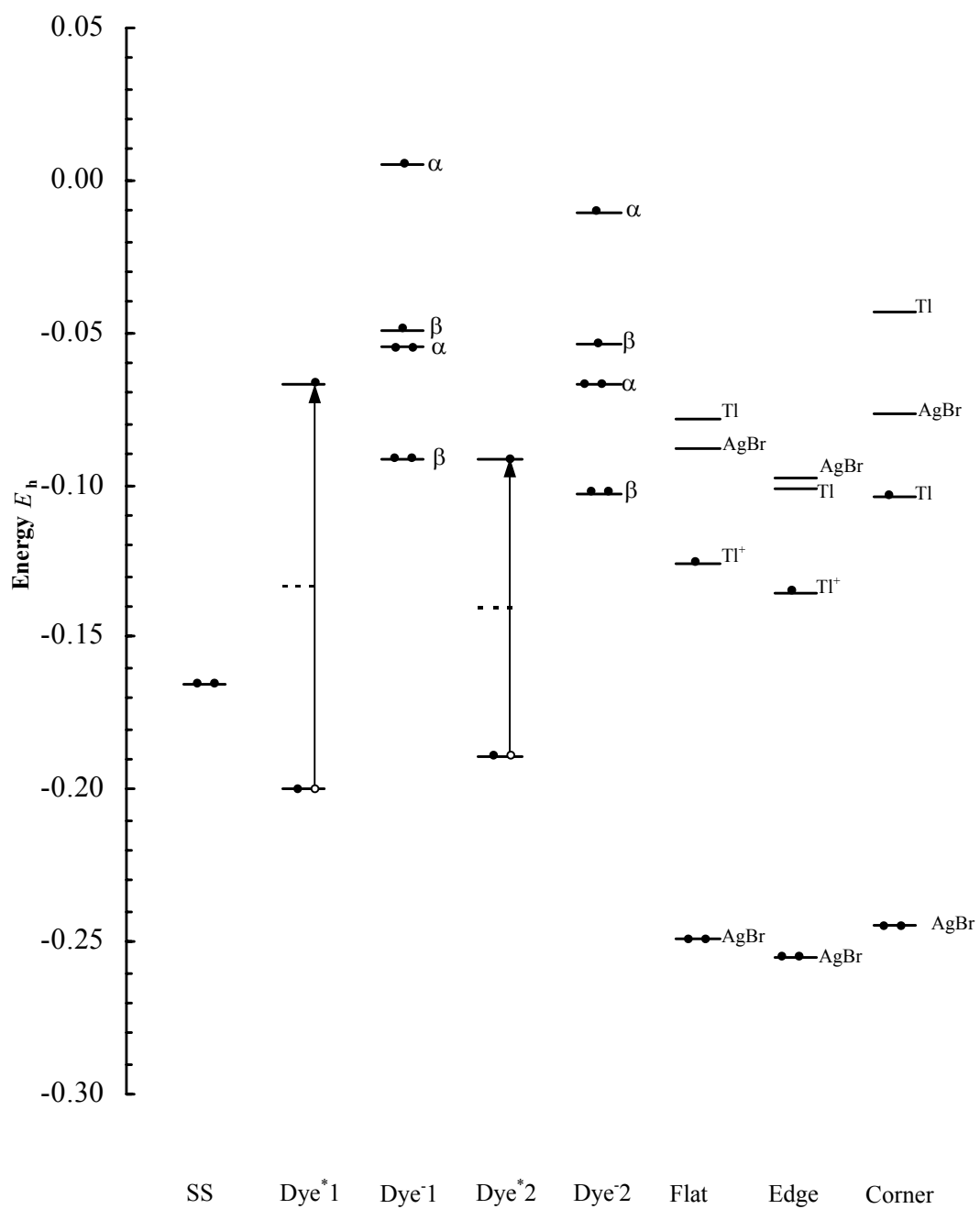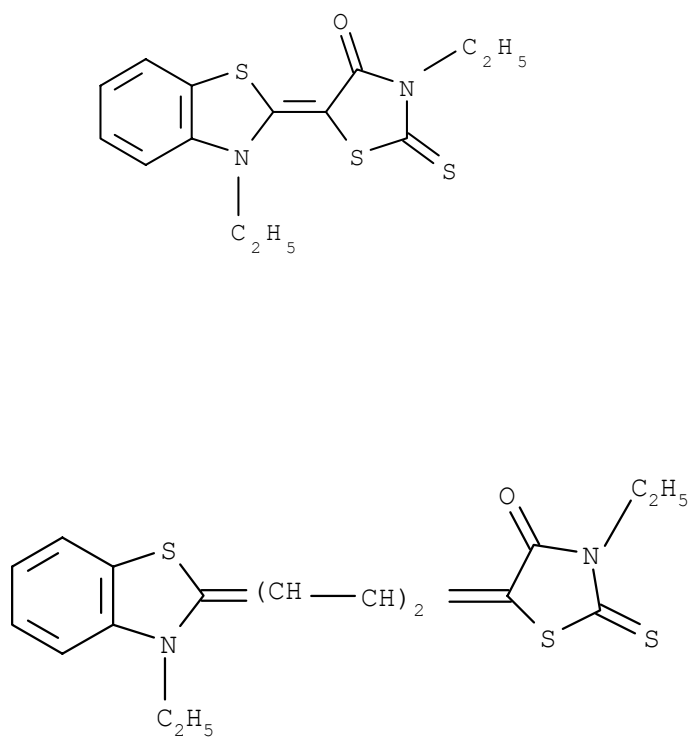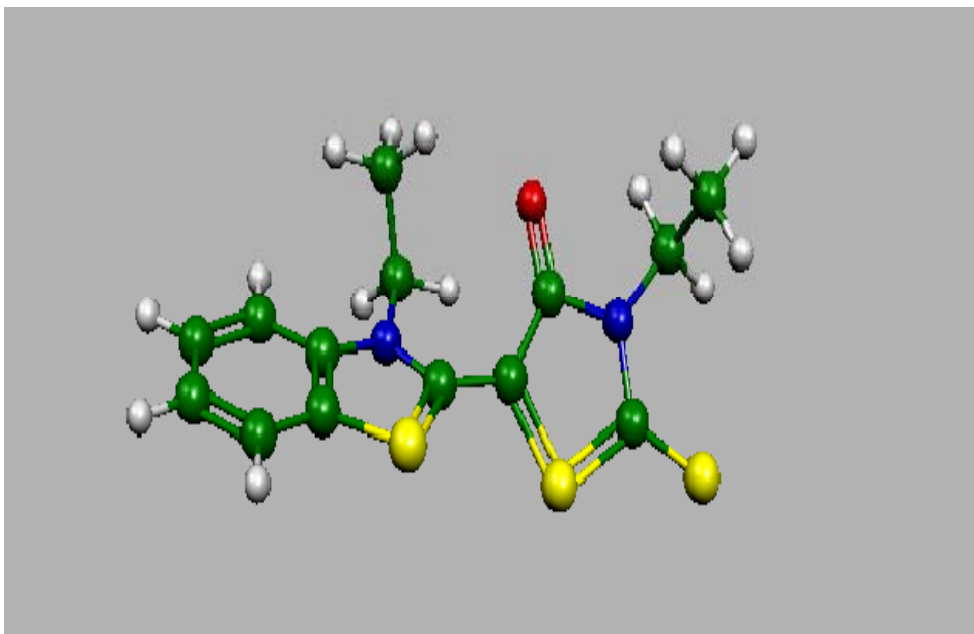**Figure (5): Diagram representing the relative energies of the ground and exited states of the low coordination surfaces of AgBr, .**
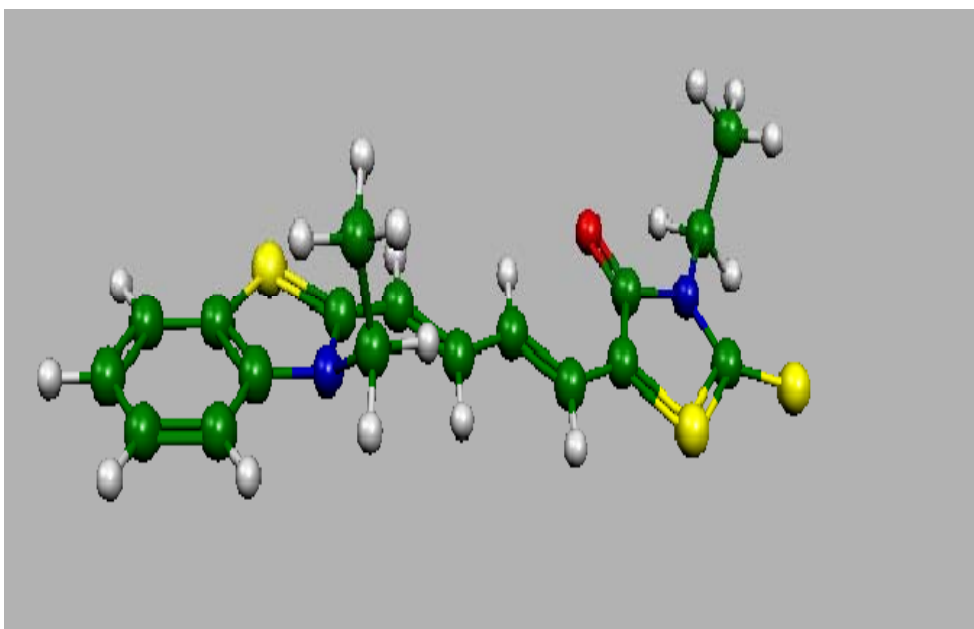
Figure (7): The electronic energy level diagarm of the dye molecules and
The AgBr surfaces.

Figure 6.a : The skeletal forms of the sensitizing dyes **1 and 2,** considered in the **calculations.**

Dye⁻ 1

Dye⁻ 2

Figure 6.b: Optimal configurations of Dye-1 and **Dye⁻ 2.**

Table 1. Specification of the finite lattices used for bulk and surface (flat, edge, and Br⁻corner) simulation of AgBr. R is half the lattice distance, which for AgBr is 2.887 Å, and r is the distance of the appropriate shell from the center of the lattice.

r^2/R^2	bulk Coordinates/R $(\pm X)\,(\pm Y)\,(\pm Z)$	Number of centers	flat Coordinates/R $(\pm X)\,(\pm Y)\,(Z \leq 0)$	Number of centers	edge Coordinates/R $(X \geq -1)\,(\pm Y)\,(Z \leq 0)$	Number of centers	Br⁻-corner Coordinates/R $(X \geq -1)\,(Y \leq 1)\,(Z \leq 0)$	Number of centers	Charge $\lvert q \rvert$
2	1 1 0	4	1 1 0	4	1 1 0	4	1 1 0	4	1
6	1 1 2	8	1 1 2	4	1 1 2	4	1 1 2	4	1
10	3 1 0	8	3 1 0	8	3 1 0	6	3 1 0	4	1
14	3 1 2	16	3 1 2	8	3 1 2	6	3 1 2	4	1
18	1 1 4	8	1 1 4	4	1 1 4	4	1 1 4	4	1
18	3 3 0	4	3 3 0	4	3 3 0	2	3 3 0	1	1
22	3 3 2	8	3 3 2	4	3 3 2	2	3 3 2	1	1
26	5 1 0	8	5 1 0	8	5 1 0	6	5 1 0	4	1
26	3 1 4	16	3 1 4	8	3 1 4	6	3 1 4	4	1
30	5 1 2	16	5 1 2	8	5 1 2	6	5 1 2	4	1
34	3 3 4	8	3 3 4	4	3 3 4	2	3 3 4	1	1
34	5 3 0	8	5 3 0	8	5 3 0	4	5 3 0	2	1
38	5 3 2	16	5 3 2	8	5 3 2	4	5 3 2	2	1
38	1 1 6	8	1 1 6	4	1 1 6	4	1 1 6	4	1
42	5 1 4	16	5 1 4	8	5 1 4	6	5 1 4	4	1
46	3 1 6	16	3 1 6	8	3 1 6	6	3 1 6	4	1
50	5 5 0	4	5 5 0	4	5 5 0	2	5 5 0	1	1
50	5 3 4	16	5 3 4	8	5 3 4	4	5 3 4	2	1
50	7 1 0	8	7 1 0	8	7 1 0	6	7 1 0	4	1
54	5 5 2	8	5 5 2	4	5 5 2	2	5 5 2	1	1
54	3 3 6	8	3 3 6	4	3 3 6	2	3 3 6	1	1
58	7 3 0	8	7 3 0	8	7 3 0	4	7 3 0	2	1
66	5 5 4	8	5 5 4	4	5 5 4	2	5 5 4	1	1
54	7 1 2	16	7 1 2	8	7 1 2	6	7 1 2	4	0.409293
62	7 3 2	16	7 3 2	8	7 3 2	4	7 3 2	2	0.409293
66	1 1 8	8	1 1 8	4	1 1 8	4	1 1 8	4	0.800909
82	9 1 0	8	9 1 0	8	9 1 0	6	9 1 0	4	0.800909
86	9 1 2	16	9 1 2	8	9 1 2	6	9 1 2	4	0.800909
		Σ=292		Σ=176		Σ=120		Σ=81	

Table (4): Energy barriers to the oriential destruction of F_B center at the low coordination surface sites of AgBr due to the migration of a bulk anion to the assumed saddle point ion configurations calculated at the CIS level. Energies are given in eV.

Flat	9.4657
Edge	7.9367
Corner	7.7595

Table (5) F_B band gap E_{FB} and exciton bands E_X at the defect containing surfaces of AgBr calculated at the DFT level. Energies are given in e.V.

	E_{FB}	E_X	E_X- E_{FB}
Flat	1.284	11.982	10.698
Edge	0.930	10.706	9.776
Corner	1.657	11.101	9.444

Table (2): Minima of the ground states (Q_1), low lying excited states (Q_2), horizontal shifts along the configurations coordinate (Q_2-Q_1), absorbed and emission transition energies ΔE between the ground states and the low lying excited states of F_B center at the low coordination surface sites of AgBr, calculated at the CIS level. All lengths are given in Å, and energies in eV.

	Q_1	Q_2	$Q_2 - Q_1$	ΔE_{abs}	ΔE_{emis}	Stokes Shift
Flat	2.5803	2.6204	0.0401	1.448	1.392	0.056
	2.3962*	2.3384*	0.0577*	1.459*	1.421*	0.038*
Edge	2.6233	2.6448	0.0215	0.810	0.797	0.013
	2.4684*	2.4106*	0.0125*	0.832*	0.820*	0.012*
Corner	2.6018	2.6161	0.0143	1.464	1.455	0.010
	2.3962*	2.3818*	0.0015*	1.473*	1.471*	0.002*

* Br basis functions are added to the Br vacancy

Table (3): The tops of valence bands (VB) and the bottoms of the conduction bands (CB) of the defect free surfaces in the ground states, and the HOMOs and LUMOs (defect levels) of the defect containing surfaces in the relaxed excited states, calculated at the CIS level. All energies are given in eV.

	Defect free surfaces ground state		Defect containing surfaces relaxed excited state	
	VB	CB	HOMOs	LUMOs[a]
Flat	-9.9752	1.0938	-5.976	-0.079
Edge	-10.1559	0.7543	-5.545	-0.413
Corner	-9.6914	1.2163	-5.4934	0.627

a Defect levels